Journal of ELECTRONIC MATERIALS, Vol. 44, No. 1, 2015
DOI: 10.1007/s11664-014-3426-5

Structural, Ferroelectric, and Electrical Properties of $NiTiO_3$ Ceramic

TRUPTIMAYEE ACHARYA[1,2] and R.N.P. CHOUDHARY[1]

1.—Department of Physics, Institute of Technical Education & Research, Siksha 'O' Anusandhan University, Khandagiri, Bhubaneswar 751030, Odisha, India. 2.—e-mail: truptiacharya18@gmail.com

The solid-state reaction route was used to prepare polycrystalline samples of $NiTiO_3$. Basic x-ray structural analysis confirmed the formation of a single-phase compound with rhombohedral crystal structure. Study of surface morphology showed that the sample had well-defined grains with uniform distribution throughout the surface. The permittivity, tangent loss, electrical modulus, conductivity, and impedance of the material were obtained over wide ranges of temperature (25°C to 500°C) and frequency (1 kHz to 1 MHz). Strong correlation between the electrical parameters and microstructure (bulk, grain boundary, nature of charge carrier, etc.) of the material has been established. The dielectric parameters are found to be independent of temperature in both low and medium temperature ranges. The temperature-dependent bulk resistance and *I–V* characteristics exhibit negative temperature coefficient of resistance behavior of the material similar to that of semiconductors. The magnetic hysteresis loop revealed that the $NiTiO_3$ ceramic displays antiferromagnetic behavior with weak ferromagnetism at room temperature. The frequency dependence of the electrical modulus and impedance of the material shows deviation from ideal Debye-type relaxation. The frequency and temperature dependence of the alternating-current (AC) conductivity and activation energy of the system obey Jonscher's universal power law with non-Debye type of relaxation. The nature of the hysteresis loop shows that the material has ferroelectric characteristics at room temperature.

Key words: X-ray structural analysis, electrical modulus, impedance

INTRODUCTION

In the microwave electronics industry, there is huge demand to develop ideal ceramic components with high quality factor, high dielectric constant/permittivity, low dielectric loss, low temperature variation of resonant frequency, etc. However, it is difficult to obtain a single-phase material with all the above properties. Recently, some single-phase titanates with general formula $ATiO_3$ (A = Ni, Fe, Co, Mn, Cu, Pb, Cd, Zn) have been developed for wide applications such as electrodes for solid-oxide fuel cells, metal–air barriers, gas sensors, and high-performance catalysts.[1–3] Recently, some materials with 3*d* transition-metal ions (substituted at the A site) have been investigated extensively due to their academic[4–6] as well as technological importance.[7–9] Though various properties of this type of material had been investigated for years, their dielectric properties were first reported in 2006.[10] $NiTiO_3$ is an important and interesting member of the $ATiO_3$ family because of its antiferromagnetic and semiconducting characteristics with a wide bandgap (3.2 eV) (as given in Table II). Therefore, it holds tremendous potential for a wide range of applications such as semiconductor rectifiers,[11] high-temperature superconductors, gas sensors,[12] etc. Fennie et al.[13] proposed a strategy to design structures based on a symmetry principle. As polar lattice distortion induces weak ferromagnetism, some magnetic perovskites such as $FeTiO_3$, $MnTiO_3$, and $NiTiO_3$ can be used as multiferroics. The Ti ions in $3d^0$ state of $NiTiO_3$ dominate the ferroelectric

(Received July 2, 2014; accepted September 16, 2014; published online October 7, 2014)

polarization, whereas Ni ions (having partially filled orbitals) are considered to contribute to the antiferromagnetic properties of $NiTiO_3$. Detailed literature survey shows that not much work on the multiferroic characteristics, beyond synthesis of $NiTiO_3$, has been reported so far. $NiTiO_3$ particles and thin films have been synthesized by different methods such as solution combustion,[14] polymeric precursor,[15] sol–gel spin coating,[16] sol–gel,[17,18] modified Pechini,[19] flux,[20] stearic acid gel,[21] coprecipitation,[22] and molten salt synthesis.[23] This motivated us to investigate the structure, dielectric properties, and magnetic properties of $NiTiO_3$ ceramic synthesized using a simple and low-cost but standard method.

EXPERIMENTAL PROCEDURES

A polycrystalline sample of $NiTiO_3$ was prepared by the standard solid-state reaction technique. Pure (>99%) fine powders of NiO (M/s HiMedia Lab) and TiO_2 (M/s Loba Chemie), taken in proper stoichiometric ratio, were thoroughly mixed in dry atmosphere (air) using a mortar and pestle for 1 h, and in wet atmosphere (methanol) for 2 h. The homogeneous mixture of the ingredients was then calcined at 1100°C for 4 h in a high-purity alumina crucible. The calcined powder of the prepared compound mixed with a small amount of polyvinyl alcohol (PVA) was pressed into pellets using a uniaxial hydraulic press at pressure of 5×10^6 N/m^2. The pellets were sintered at 1150°C for 4 h in air atmosphere. The phase formation with basic crystal data of the sample was determined using x-ray diffraction (XRD) data collected by diffractometer (D8 Advance; Bruker) at room temperature over a wide range of Bragg angle θ ($20° \le 2\theta \le 80°$) at scan rate of 3°/min. The micrograph of the sintered pellet was recorded by scanning electron microscopy (SEM). For electrical characterization, a thin layer of highly conducting silver paint was coated on both sides of the sintered sample, followed by heat treatment at 150°C for 45 min. An impedance analyzer (phase-sensitive meter) was used to measure the impedance and related parameters over a wide frequency range (1 kHz to 1 MHz) at different temperatures (room temperature to 500°C). The hysteresis loop of the poled sample was traced using a *P–E* hysteresis loop tracer (M/s Marine India Co.) at different temperatures. The current–voltage characteristics of $NiTiO_3$ were measured at intervals of 25°C in the temperature range from 25°C to 500°C using a programmable electrometer (model 6517B; Keithley).

RESULTS AND DISCUSSION

Structural and Microstructural Analysis

Figure 1 shows the room-temperature XRD pattern of $NiTiO_3$. All the peaks of the XRD pattern were indexed using PowdMult standard computer software.[24] On heating the pellet sample from 1100°C to higher temperatures, the sharpness and intensity of

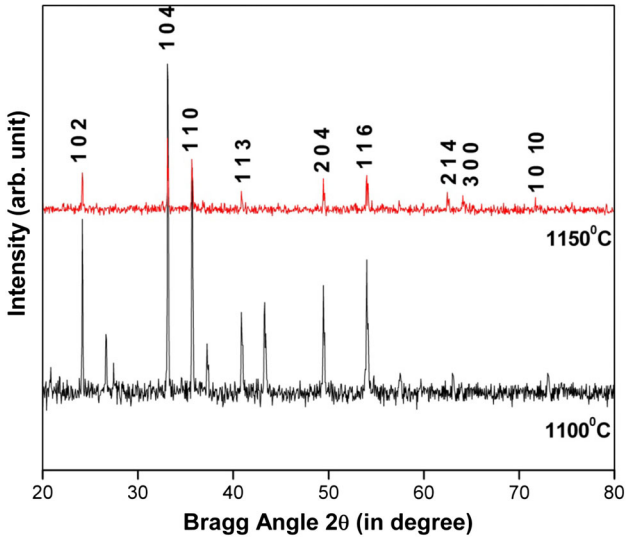

Fig. 1. X-ray diffraction pattern of $NiTiO_3$ powder at room temperature.

the XRD peaks of the sample increased (Fig. 1). Based on the minimum value of the difference between the observed (obs) and calculated (cal) interplanar spacing ($d_{obs} - d_{cal}$ = minimum), a rhombohedral crystal system was selected, in accordance with earlier reports.[22,25] The lattice parameters (obtained from the above calculations) were refined using the least-squares refinement subroutine of PowdMult. The least-squares refined unit cell parameters are: a = 5.0294 Å, c = 13.7947 Å, c/a = 2.7428, and V = 302.18 Å^3 (with estimated standard deviation of the unit cell parameters of 0.011 Å). The crystallite size (P) of $NiTiO_3$ was estimated from the peak broadening $\beta_{1/2}$ (peak width at half-height) and peak position (2θ) of some higher-angle reflections using Scherrer's relation,[26] $P = k\lambda/\beta_{1/2}\cos\theta$ (k = constant = 0.89, λ = 0.15407 nm). The value of the crystallite size was found to be 61 nm. Broadening due to strain, the instrument, and other sources was ignored in the calculation of P. The crystallite size of $NiTiO_3$ synthesized by the molten salt method was reported to be 70 nm,[23] and for the wet chemical method it was reported to be 65 nm (for high calcination temperature).[27] The crystallite size of $NiTiO_3$ synthesized by the solid-state reaction method is highly consistent with values reported earlier.

Figure 2 shows a SEM micrograph of the sintered pellet. It is observed that grains of different dimensions and shapes are uniformly distributed (with small voids) over the entire surface of the sample. The grain size was found to be in the range of 3 μm to 10 μm.

Dielectric Studies

Frequency-Dependent Dielectric Parameters

The dielectric constant (permittivity) is one of the basic electrical properties of insulators. Measurement of the dielectric constant and tangent loss as a

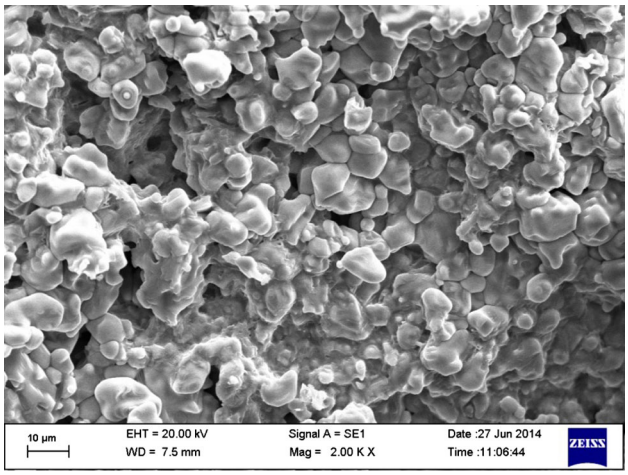

Fig. 2. SEM micrograph of $NiTiO_3$ at room temperature.

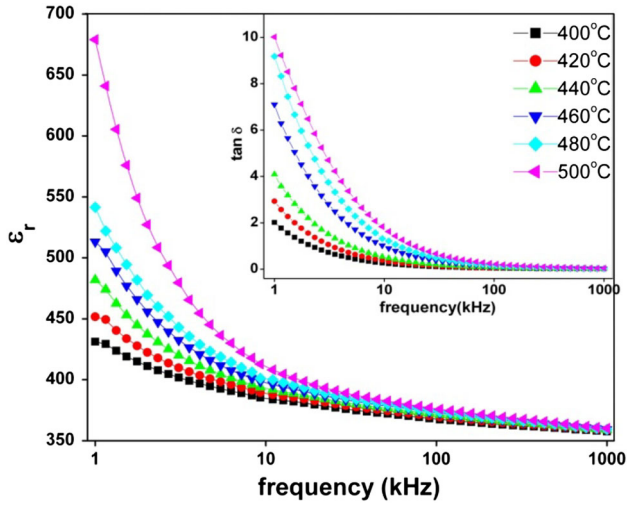

Fig. 3. Variation of relative dielectric constant (ε_r) with frequency at different temperatures for $NiTiO_3$. Inset shows variation of tangent loss (tan δ) as a function of frequency.

function of frequency and temperature is of great interest from both a theoretical as well as practical point of view. Practically, the presence of a dielectric between the plates of a capacitor/condenser enhances the capacitance of the material. Essentially, the relative dielectric constant (ε_r) is a measure of how easily a material is polarized in an external electric field. The dependence of the dielectric constant (ε) and tangent loss (tan δ) on the frequency of an applied AC field was studied over a wide temperature range (25°C to 500°C) at different frequencies (1 kHz to 1 MHz) on a pellet sample (diameter 0.16 cm, thickness 0.92 cm). The dielectric constant was found to lie within the range of 553 to 679. Because of the moderately high value of the dielectric constant, $NiTiO_3$ can be considered a high-k dielectric useful for nonvolatile ferroelectric random-access memory (FeRAM).

Figure 3 shows the variation of the dielectric constant and loss tangent as a function of frequency in the temperature range from 400°C to 500°C. The dielectric constant decreases rapidly with increasing frequency in the lower frequency range, and appears to attain its saturation limit for frequencies greater than 10^3 kHz. This behavior of $NiTiO_3$ ceramic is exactly similar at all temperatures applied in the experiment (i.e., 25°C to 500°C). This suggests that the material can be used as a lossless material in transistors, microelectronic devices, etc. Though a similar trend for the variation of the dielectric constant of $NiTiO_3$ was reported earlier,[27,28] those values were found to be relatively lower as compared with the present study. The variation of the dielectric constant and loss tangent with frequency at different temperatures may be attributed to different types of polarization (viz. ionic, electronic, dipolar, and interfacial or space charge). Each type of polarization involves a short-range displacement of charges and contributes to the total polarization and thus to the dielectric constant of the material. It is a well-known fact that the contribution of dipolar polarization and space-charge polarization is most significant at lower frequencies.[29] Hence, the dielectric constant is high in the low-frequency region. At higher frequencies, the contribution of space-charge and other polarization is zero or negligibly small, and only the electronic polarization contributes to the dielectric constant. Therefore, the value of the dielectric constant is lower at higher frequencies. Further, a continuous decrease of the dielectric constant with increasing frequency occurs because dipoles are not able to follow faithfully the applied oscillating field. The loss tangent decreases in the same manner as the dielectric constant. As both dielectric parameters appear to decrease with increasing frequency, this indicates a normal behavior of the compound having mobile carriers.[30]

Temperature-Dependent Dielectric Parameters

Figure 4 shows the variation of the relative dielectric constant (ε_r) and loss tangent as a function of temperature at some selected frequencies (1 kHz to 10^3 kHz). From the plot of the dielectric constant (ε_r) versus temperature it can be seen that the value of the dielectric constant is almost constant up to 200°C. This value is independent not only of temperature but also of frequency, which indicates that the intrinsic dielectric response is due to the electronic and/or ionic polarization. Above 200°C, the dielectric constant exhibits a weak stepwise increase up to 350°C with further rise in temperature, and beyond 350°C, ε_r exhibits a sharp increase up to 500°C; thus there is a maximum value at 500°C, which is consistent with previous report.[29] The sharp increase in the above parameters may be due to scattering of thermally activated charge carriers or may be due to some defects in the

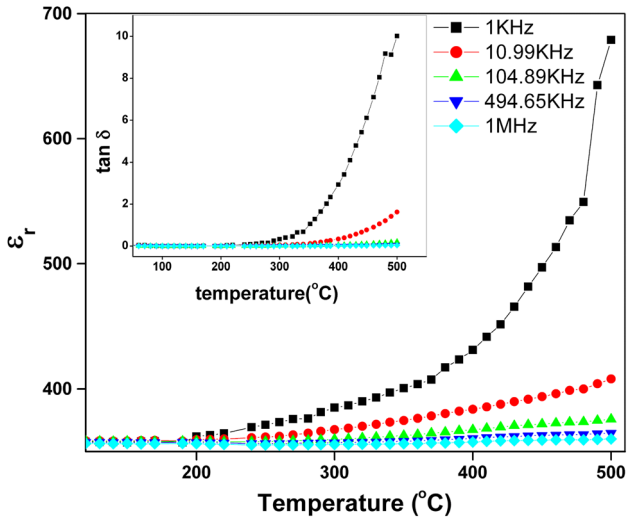

Fig. 4. Variation of relative dielectric constant and tangent loss with temperature at different frequencies for $NiTiO_3$.

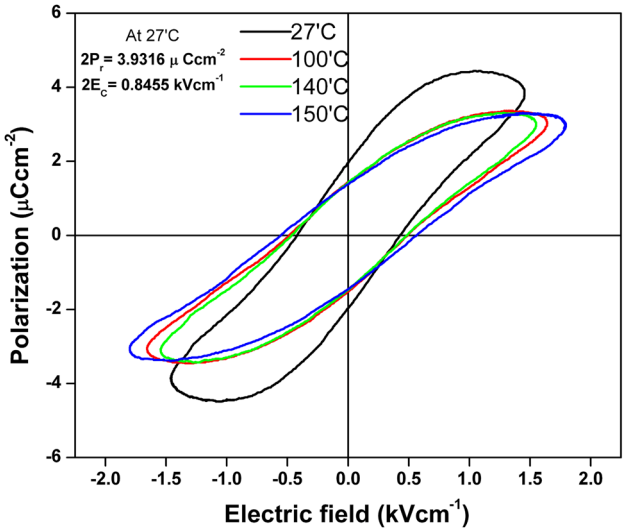

Fig. 5. Comparison of hysteresis loops recorded at different temperatures for $NiTiO_3$.

samples.[31] The tangent loss also shows an almost constant value up to 200°C, then increases with rise in temperature.

Polarization Study

The reported ferroelectric properties of $NiTiO_3$ at room temperature were reinvestigated by recording the polarization (P) versus electric field (E) characteristic of our pellet sample. Figure 5 shows the hysteresis loop of $NiTiO_3$ at different temperatures. The existence of a hysteresis loop in the low-temperature region confirms the ferroelectricity of the material. The remnant polarization ($2P_r$) of $NiTiO_3$ at room temperature is found to be 3.932 $\mu C/cm^2$ at coercive field of 0.85 kV/cm. It is seen that, with increasing temperature, the remnant polarization decreases. This decrease in P_r with rise in temperature is due to the presence of bound charges, which are randomized with increase in temperature.[31] The nature of the hysteresis loop of the material is largely normal except for some anomalies in the polarization (i.e., the maximum value of the polarization is slightly higher than the saturation polarization, and the asymmetric shape). There could be various reasons for these anomalies, including (i) influence of electrode at the microscopic level, (ii) nonuniform polarization due to polarization gradient, (iii) induced polarization, and (iv) inhomogeneous domains created in/on the sample surface.[32] The phase-transition temperature of the compound is far above room temperature (i.e., 500°C).[28] Therefore, the transition temperature is also expected to be high. As it was not possible to reach the expected high temperature to confirm the ferroelectric–ferromagnetic phase transition with the existing experimental facilities, some of the hysteresis loops recorded up to temperature of 150°C are presented herein.

Impedance and Modulus Spectroscopy

Background and Results

Complex impedance spectroscopy (CIS) is a well-known technique to study the electrical properties of ionic and ceramic materials as a function of frequency and temperature. The grain and grain boundary contributions to the electrical response of dielectric materials can be well analyzed using this technique. The frequency dependence of physical properties of materials can be described via the complex dielectric permittivity (ε^*), complex impedance (Z^*), complex admittance (Y^*), and dielectric loss (tan δ). These parameters are related to each other by the following relations:

$$\text{Complex impedance: } Z^* = Z' - jZ'' = R_s - (j/\omega C_s), \quad (1)$$

$$\text{Complex modulus: } M^*(\omega) = 1/\varepsilon(\omega) = M' + jM'' = j\omega C_0 Z^*, \quad (2)$$

$$\text{Complex admittance: } Y^*(\omega) = Y' + jY'' = j\omega C_0 \varepsilon^* = (R_p)^{-1} + j\omega C_p, \quad (3)$$

$$\text{Complex dielectric permittivity: } \varepsilon^* = \varepsilon' - j\varepsilon'', \quad (4)$$

$$\text{Tangent loss : } \tan\delta = \varepsilon''/\varepsilon' = M''/M' = -Z'/Z'', \quad (5)$$

where the angular frequency is $\omega = 2\pi f$, the geometrical capacitance is $C_0 = \varepsilon_0 A/t$, and the

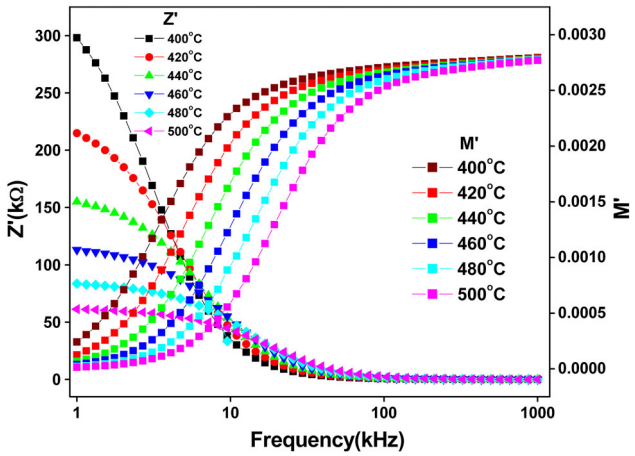

Fig. 6. Variation of Z' and M' with frequency for $NiTiO_3$ at different temperatures.

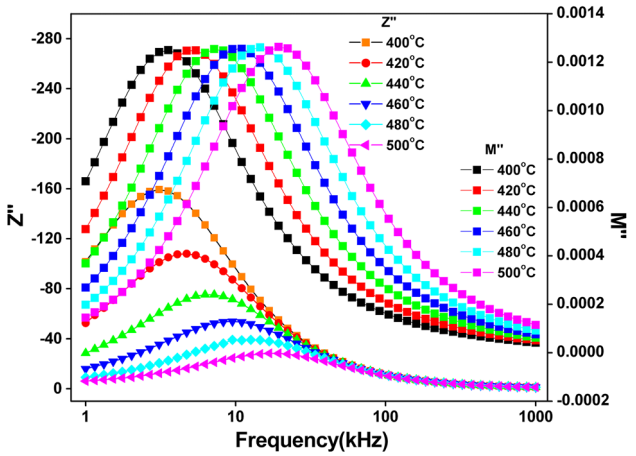

Fig. 7. Variation of Z'' and M'' with frequency for $NiTiO_3$ at different temperatures.

subscripts "p" and "s" indicate parallel and series, respectively.The relaxation frequency, ω_{max}, of the bulk material can be calculated using the relation: $\omega_{max}\tau = \omega_{max}R_bC_b = 1 = 2\pi f_{max}R_bC_b$, where R_b is the bulk resistance and C_b is the bulk capacitance.

Figure 6 shows the variation of Z' and M' with frequency at high temperatures (i.e., 400°C to 500°C). It is observed that Z' decreases with increase in frequency and temperature. This plot also shows that the conductivity increases with rise in temperature. It shows dispersion at low frequencies. At higher frequencies, all the curves merge into one, indicating the release of space charge, which eventually increases the conductivity. At lower frequencies, it is seen that M' is nearly zero. Then, there is a continuous increase in its value with further increase in the frequency. The plots show a tendency to saturate at a maximum asymptotic value in the high-frequency region for all temperatures. This is attributed to the presence of conduction phenomena arising due to the short-range mobility of charge carriers.[33]

Figure 7 shows the variation of Z'' and M'' with frequency at different temperatures. The values of these parameters increase initially, attain a peak value (Z''_{max}), then decrease with frequency at all measured temperatures. The dispersion of the curves for Z'' appears to merge at higher frequencies. This is due to the absence of space-charge polarization at higher frequencies. With increasing temperature, the Z''_{max} peak decreases, indicating relaxation in the samples. It is seen that the Z'' and M''_{max} peaks broaden with increasing temperature, indicating relaxation with different time constants and suggesting the occurrence of non-Debye type of relaxation in the material. Such relaxation may be due to (i) defects and oxygen ion vacancies at high temperatures and (ii) presence of immobile ions at low temperatures.[28,29] The Z''_{max} and M''_{max} peaks shift towards higher frequency with increasing temperature, indicating a decrease in the relaxation time with increasing temperature. This combined plot is useful to find the effect of the smallest capacitance and the largest resistance, which helps to distinguish whether a relaxation process is due to long- or short-range mobility of charge carriers. If the process is of short-range type, the peaks of Z''_{max} and M''_{max} do not occur at the same frequency. If the process is of long-range type, the peaks occur at the same frequency.[34,35] As there is a mismatch between the peaks of Z'' and M'', the relaxation in the material may be considered to be of non-Debye type due to short-range mobility of charge carriers.

Analysis of Impedance Spectra

Figure 8 shows the complex impedance spectra (usually referred to as the Nyquist plot) at different temperatures in the frequency range from 1 kHz to 1 MHz. It is found that the impedance decreases with rise in temperature, exhibiting the temperature dependence of conductivity of the material. For Debye-type relaxation, a perfect semicircle should be observed (with center on the Z' axis). However, these figures exhibit depressed semicircles with center depressed below the Z' axis, suggesting deviation from ideal Debye-type behavior.[36,37] The intercept of the first semicircle with the Z' axis gives the value of the bulk resistance, and the second semicircle gives the grain boundary contribution. As can be seen from the figure, a single semicircle is observed in the high-frequency region. This arc is associated with the bulk conduction of the material. This behavior is due to the contribution of the parallel combination of both the bulk capacitance C_b and bulk resistance R_b (shown as the inset of Fig. 8) due to the electric relaxation phenomena. Each semicircle corresponding to each temperature has its own relaxation frequency, thus the relation connecting the relaxation time (τ) with the applied frequency is given by

$$\tau = \frac{1}{\omega} = R_bC_b, \quad (6)$$

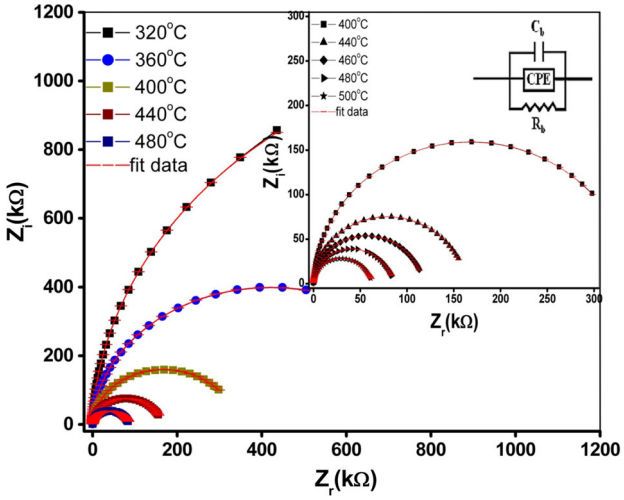

Fig. 8. Variation of Z' with Z'' for $NiTiO_3$ at different temperatures along with the equivalent circuit.

where $\omega = 2\pi f_{max}$, and f_{max} is the applied frequency corresponding to the arc maximum. In the low-frequency region, there is no semicircle, which indicates that grain boundaries do not contribute to the impedance or electrical parameters; only bulk conduction occurs in the material. The diameter of the semicircle, as obtained by the intercept of the semicircle with the x-axis, gives the value of the bulk resistance R_b. The experimental values were fit to an equivalent circuit model using the software ZSimpWin version 2, confirming the accuracy of the experimental data.

The electrical conduction mechanism in metal titanates is due to oxygen vacancies, which are the mobile charge carriers (ionization creates conduction electrons). The excess electrons and the oxygen vacancies are formed via the following reduction reaction[38]:

$$O_0^x \rightarrow \frac{1}{2}O_2(g) + V_0^x, \tag{7}$$

$$V_0^x \rightarrow V^* + e', \tag{8}$$

$$V_0^x \leftrightarrow V^{**} + e'. \tag{9}$$

Doubly charged oxygen vacancies are considered to play an important role in conduction in these oxides.

$$O_0^x \rightarrow \frac{1}{2}O_2(g) + V_0^{**} + 2e. \tag{10}$$

These electrons are responsible for the space-charge polarization, thus enhancing the conductivity when thermally activated. Excess electrons so formed can bond with Ti^{4+} to form Ti^{3+}.[38]

AC Conductivity

Figure 9 shows the variation of the AC conductivity with frequency at higher temperatures (380°C to 500°C). At lower temperatures, the conductivity increases with increase in frequency, corresponding to an ω^n characteristic (n = exponent). At higher temperatures and low frequencies, the conductivity shows a flat response, while it exhibits ω^n dependence at high frequencies. The AC conductivity was calculated using some dielectric data via the relation[39]

$$\sigma_{AC} = \omega\varepsilon_r\varepsilon_0 \tan\delta, \tag{11}$$

where ω is the angular frequency, ε_r is the relative dielectric constant, ε_0 is the permittivity of free space, and $\tan\delta$ is the tangent loss. Jonscher's power law can successfully be applied by knowing the variation of the AC conductivity (with frequency) using the equation[40]

$$\sigma_T(\omega) = \sigma(0) + \sigma_1(\omega) = \sigma_0 + A\omega^n, \tag{12}$$

where $\sigma_T(\omega)$ is the total conductivity, $\sigma(0)$ is the direct-current (DC) conductivity term (independent of frequency), and $\sigma_1(\omega)$ is the dispersive component of the AC conductivity. A and n are frequency- and temperature-dependent parameters. A determines the magnitude of the dispersion, and the value of n lies between 0 and 1. For an ideal capacitor $n = 1$, and for an ideal resistor $n = 0$.[23] The calculated values of R_b, C_b, and n are listed in Table I. The value of the bulk capacitance was calculated using the relation $2\pi f_{max}R_bC_b = 1$, being on the order of picofarads (pF). The high capacitance value shows that the conduction is through the bulk of the material. The relaxation time τ was calculated by using Eq. 6. The value of the relaxation time at different temperatures is given in Table I, and it is noted that the relaxation time decreases with increase in temperature, indicating that the diffusion of the carriers is a thermally activated phenomenon. The longer the relaxation time, the slower the relaxation process. The relaxation time relies only on the structural/microstructural properties of the material. According to Jonscher,[41] the origin of the frequency dependence of the conductivity lies in the relaxation phenomena arising due to mobile charge carriers. When a mobile charge carrier hops to a new site from its original site, it remains in a state of displacement between two potential energy minima. Also, the conduction behavior of the material obeys the power law $\sigma(\omega) \propto \omega^n$ with a slope change governed by n in the low-temperature region. A value of $n < 1$ signifies that the hopping process involves translational motion with sudden hopping of charge carriers, whereas $n > 1$ means that the motion involves localized hopping without the species leaving the neighborhood.[42] The frequency at which the change in slope takes place is known as

the hopping frequency of polarons (ω_p), being temperature dependent. The high-frequency dispersion has been attributed to the AC conductivity, whereas the frequency-independent plateau region corresponds to the DC conductivity. The material obeys universal power laws, as confirmed by fitting the above equation to the experimental data (also shown in Fig. 9). From the nonlinear fitting it is found that the motion of the charge carriers is translational because of the small value of n (<1). (The values of n are given in Table I.)

Figure 10 shows the variation of the AC conductivity with the inverse of the absolute temperature at different frequencies. At 25°C, the conductivity is found to be $1.03 \times 10^{-6}\ \Omega^{-1}\ m^{-1}$, whereas at 500°C it is $3.77 \times 10^{-4}\ \Omega^{-1}\ m^{-1}$. This shows that, with rise in temperature, the AC conductivity increases drastically, suggesting that the material exhibits negative temperature coefficient of resistance (NTCR) behavior. At higher temperatures, all the conductivity curves at the different frequencies tend to merge, indicating frequency-independent behavior in this region.

DC Conductivity

The DC electrical conductivity was calculated using the relation $\sigma_{DC} = t/SR_b$, where t and S are the thickness and area of the sample, respectively, and R_b is the bulk resistance. Figure 11 shows the variation of the DC conductivity with inverse temperature for the $NiTiO_3$ ceramic sample. The following Arrhenius relation can be used to calculate the DC conductivity:

$$\sigma_{DC} = \sigma_0 \exp(-E_a/k_B T), \tag{13}$$

where k_B is the Boltzmann constant, σ_0 is the pre-exponential factor, and E_a is the activation energy of the mobile charge carriers. The activation energy (bulk) for the sample was estimated to be 0.79 eV for the high-temperature region, demonstrating that a small amount of energy is sufficient to activate the charge carriers for electrical conduction. The slope of the curve was estimated by using a linear fit. It is seen that, with rise in temperature, the DC conductivity increases, indicating that the conduction is via a thermally activated process. This shows that

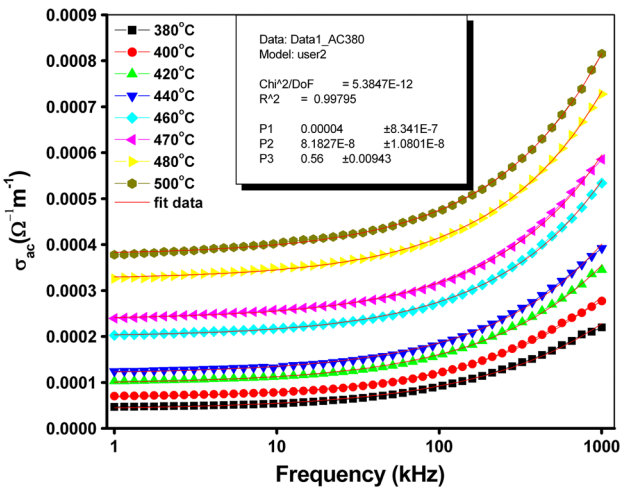

Fig. 9. Variation of AC conductivity of $NiTiO_3$ with frequency at different temperatures.

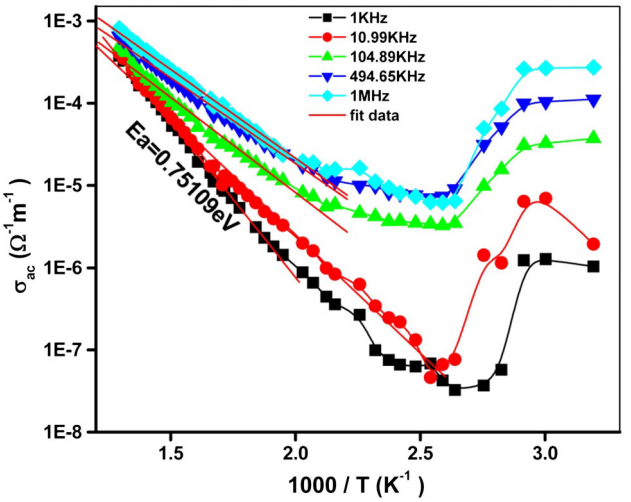

Fig. 10. Variation of AC conductivity of $NiTiO_3$ with inverse absolute temperature at different frequencies.

Table I. Values of R_b, C_b, σ_{DC}, σ_0, τ, and n for $NiTiO_3$ ceramic at different temperatures

Temp. (°C)	$R_b \times 10^5$ (ohm)	C_b (pF)	σ_{DC} (S cm^{-1})		σ_0 (S cm^{-1})	Relaxation Time, τ (s)	n
			Nyquist Plot	Conductance			
380	5.19100	132.4	4.50707×10^{-5}	0.00004	5.87×10^{1}	6.87288×10^{-5}	0.56
400	3.43200	132.7	6.81707×10^{-5}	0.00006	5.55×10^{1}	4.55426×10^{-5}	0.58212
420	2.35000	133.9	9.95583×10^{-5}	0.0001	5.48×10^{1}	3.14665×10^{-5}	0.60558
440	1.64300	133.9	1.42399×10^{-4}	0.00012	5.41×10^{1}	2.19998×10^{-5}	0.62164
460	1.18300	134.3	1.9777×10^{-4}	0.0002	5.29×10^{1}	1.58877×10^{-5}	0.65051
480	0.8654	134.9	2.70351×10^{-4}	0.00028	5.19×10^{1}	1.16223×10^{-5}	0.65712
500	0.6445	135.6	3.63013×10^{-4}	0.00038	5.08×10^{1}	8.73942×10^{-6}	0.65437

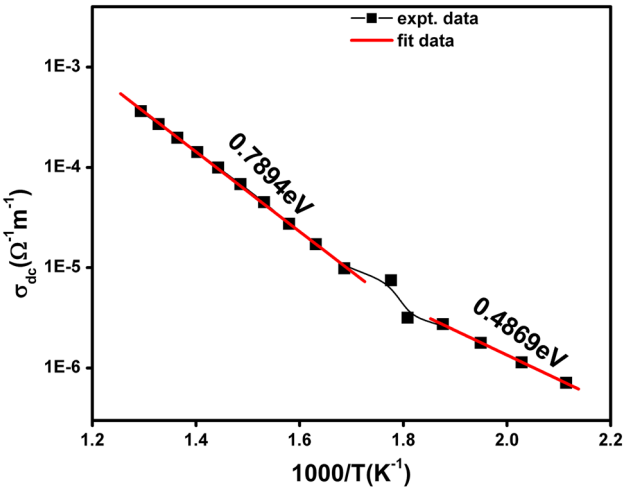

Fig. 11. Variation of DC conductivity with inverse absolute temperature.

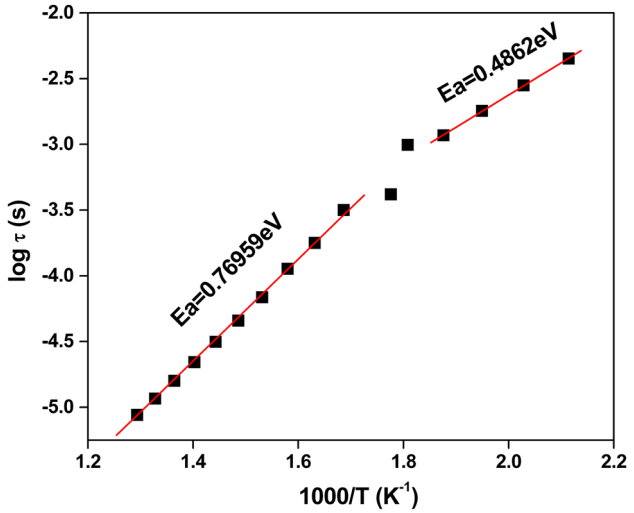

Fig. 12. Variation of relaxation time with inverse absolute temperature.

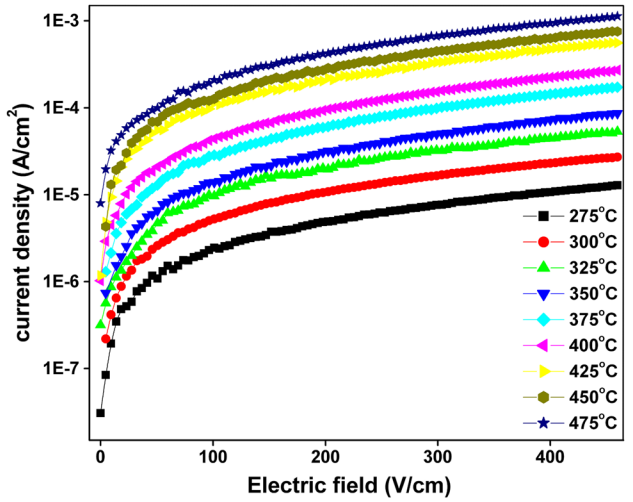

Fig. 13. Variation of current density with electric field.

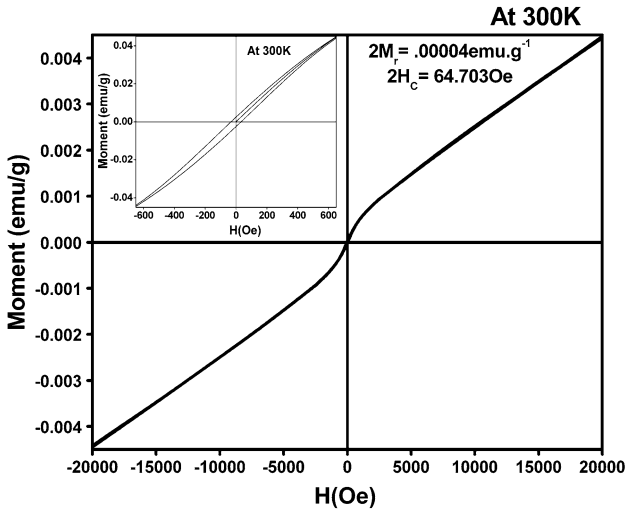

Fig. 14. Variation of magnetic moment (M) with magnetic field (H) for $NiTiO_3$ at room temperature.

$NiTiO_3$ exhibits semiconducting behavior. According to Davis and Mott,[43] the activation energy alone does not indicate that the conductivity mechanism involves extended states above the mobility edge or by hopping in localized states or due to the effect of impurities or defects. A distinction between these mechanisms can be drawn on the basis of the value of the pre-exponential factor (σ_0). It was suggested by Mott[43] that the pre-exponential factor (σ_0) for conduction in localized states should be two or three orders smaller in magnitude than for conduction in extended states and should become still smaller for conduction in localized states near the Fermi level. The value of the pre-exponential factor (σ_0) in the range of $10^3\ \Omega^{-1}\ cm^{-1}$ to $10^4\ \Omega^{-1}\ cm^{-1}$ indicates that the conduction is mostly in extended states. A smaller value of the pre-exponential factor (σ_0) indicates a wide range of localized states and conduction by hopping. In the present system, the values of the pre-exponential factor (σ_0) are in the range of $10^1\ \Omega^{-1}\ cm^{-1}$. (The value of σ_0 is listed in Table I.) Therefore, the possibility of extended state conduction is completely ruled out, and localized state conduction (by hopping) in the band tail is most likely.

Figure 12 shows the variation of ln τ_b with the inverse of the absolute temperature. With rise of temperature, τ_b decreases. From the relaxation-time plot, the activation energy is calculated to be 0.77 eV.

Leakage Current Characteristics

Figure 13 exhibits the leakage current of $NiTiO_3$. I–V characteristic curves of the material were obtained in the temperature range from 275°C to

Table II. Comparison of properties of $NiTiO_3$, $MnTiO_3$, and $FeTiO_3$

Property	$FeTiO_3$	$MnTiO_3$	$NiTiO_3$
Bandgap (eV)	2.54[45]	3.18[48]	3.2[26]
Coercivity (at 300 K) (Oe)	12[46]	–	32
Remnant magnetization (emu/g)	–	0.0014[47]	0.002
Resistivity (for 150°C to 300°C) (Ω m)	~0[44]	1.76×10^5[49]	7.8×10^6–1.4×10^5
Activation energy (eV)	0.21[50]	0.05[49]	0. 4869

475°C on a pellet sample with diameter of 0.97 cm and thickness of 0.218 cm. It is observed that, at all the temperatures, the value of J increases with increasing E. We also observed an increment in leakage current with increasing temperature, which confirms the thermally assisted conduction process of the material. The increase in the current density with rise in electric field is nonlinear, which suggests non-Ohmic characteristics of the above system.

Magnetic Properties

Figure 14 exhibits the M–H hysteresis loop of $NiTiO_3$ measured at room temperature. The hysteresis loop does not show a tendency for saturation with increasing applied magnetic field. The opening of the hysteresis loop is not prominent for this sample. The nature of the curve exhibits field-dependent alignment of canted spins in this material. At room temperature, antiferromagnetic behavior with weak ferromagnetism was observed in the sample, with coercive field (H_C) of 32.39 Oe and remnant magnetization (M_r) of 0.002 emu/g. The coercivity and remnant magnetization of $NiTiO_3$ ceramics are found to be higher than those reported for other members of the $ATiO_3$ family (as shown in Table II). As $NiTiO_3$ shows magnetic and semiconducting behavior, this material can be exploited for devices in which both are needed. One such application is the varistor, which is a device used for limiting transient voltage surges in a circuit. A varistor is an electronic component with a "diode-like" nonlinear current–voltage characteristic. Varistors are often used to protect circuits against excessive transient voltages by incorporating them into the circuit in such a way that, when triggered, they will shunt the current created by the high voltage away from sensitive components.[44]

CONCLUSIONS

A polycrystalline sample of $NiTiO_3$ was fabricated by the standard solid-state reaction method. In the present work, we report the detailed structural, electrical, and magnetic properties of $NiTiO_3$. XRD analysis of $NiTiO_3$ showed a rhombohedral crystal structure. The dielectric parameters of the compound strongly depend on the working temperature and frequency. The surface morphology of the compound, studied by SEM, shows homogeneously distributed grains. The compound has low tangent loss even at 500°C (0.06 at 500 kHz), which decreases with increasing frequency. Due to the low tangent loss, the quality factor of the material is high, which is a criterion for many applications including microwave devices. The nature of the variation of the permittivity and the appearance of a hysteresis loop at room temperature confirm the reported ferroelectricity in this material. The complex impedance plots reveal that the material exhibits (i) electrical transport (conduction) due to bulk material, (ii) negative temperature coefficient of resistance (NTCR) behavior, and (iii) temperature-dependent relaxation phenomenon. Complex impedance analysis suggests that the dielectric relaxation in the material is of polydispersive, non-Debye type. The frequency dependence of the AC conductivity obeys Jonscher's universal power law. The activation energy for the sample calculated from the DC conductivity is estimated to be 0.79 eV and from the relaxation plot is calculated to be 0.77 eV. The values of E_a calculated by these two different methods are very similar. This indicates that similar types of charge are responsible for relaxation and conduction in this material. The magnetic measurements show antiferromagnetic behavior with weak ferromagnetism for $NiTiO_3$. The J–E characteristics suggest a non-Ohmic nature of $NiTiO_3$. Thus, the present study indicates that $NiTiO_3$ exhibits semiconducting behavior along with a magnetic nature, which could be exploited for devices such as varistors in which both are needed. Since $NiTiO_3$ exhibits ferroelectricity and also shows antiferromagnetism, there may be magnetoelectric coupling in $NiTiO_3$. Hence, there is a possibility that $NiTiO_3$ is a multiferroic material, which could be very useful for multifunctional devices such as spintronics, etc.

ACKNOWLEDGEMENTS

The authors are grateful to Miss Harapriya Rath of Utkal University, Vani Vihar, Bhubaneswar for her kind help in some experiments.

REFERENCES

1. N. Dharmaraj, H.C. Park, C.K. Kim, H.Y. Kim, and D.R. Lee, *Mater. Chem. Phys.* 87, 5 (2004).
2. T. Kazuyuki, U. Yasuo, T. Shuji, I. Takashi, and U. Akifumi, *J. Am. Chem. Soc.* 106, 5172 (1984).
3. D.U. Kim and M.S. Gong, *Sens. Actuators B Chem.* 110, 321 (2005).

4. J.J. Stickler and G.S. Heller, *J. Appl. Phys.* 33, 1302 (1962).
5. G.S. Heller, J.J. Stickler, S. Kern, and A. Wold, *J. Appl. Phys.* 34, 1033 (1963).
6. J.B. Goodenough and J.J. Stickler, *Phys. Rev.* 164, 785 (1967).
7. X.F. Chu, X.Q. Liu, G.Z. Wang, and G.Y. Meng, *Mater. Res. Bull.* 34, 1789 (1999).
8. M.S. Sadjadi, M. Mozaffari, M. Enhessari, and K. Zare, *Superlattices Microstruct.* 47, 685 (2010).
9. C.L. Huang, J.Y. Chen, and G.S. Huang, *J. Alloys Compd.* 499, 48 (2010).
10. P.S. Anjana and M.T. Sebastian, *J. Am. Ceram. Soc.* 89, 2114 (2006).
11. H. Wendt and G. Imarisio, *J. Appl. Electrochem.* 18, 1 (1988).
12. H. Wendt and G. Imarisio, *J. Solid State Chem.* 17, 299 (1976).
13. C.J. Fennie, *Phys. Rev. Lett.* 100, 167203 (2008).
14. Y. Ni, X. Wang, and J. Hong, *Mater. Res. Bull.* 44, 1797 (2009).
15. K.P. Lopes, L.S. Cavalcante, A.Z. Simoes, J.A. Varela, E. Longo, and E.R. Leite, *J. Alloys Compd.* 468, 327 (2009).
16. A.R. Phani and S. Satucci, *Thin Solid Films* 396, 1 (2001).
17. D.Y. Taylor, P.F. Fleig, and R.A. Page, *Thin Solid Films* 408, 104 (2002).
18. S. Chuang, M. Hsieh, S. Wu, H. Lin, T. Chao, and T. Hou, *J. Am. Ceram. Soc.* 94, 250 (2011).
19. Y. Lin, Y. Chang, W. Yang, and B. Tsai, *J. Non-Cryst. Solids* 352, 789 (2006).
20. R.S. Singh, T.H. Ansari, R.A. Singh, and B.M. Wanklyn, *Mater. Chem. Phys.* 40, 173 (1995).
21. M.S. Sadjadi, K. Zare, S. Khanahmadzadeh, and M. Enhessari, *Mater. Lett.* 62, 3679 (2008).
22. A. Vadivel Murugan, V. Samuel, S.C. Navale, and V. Ravi, *Mater. Lett.* 60, 1791 (2006).
23. S. Yuvaraj, V.D. Nithya, K. Saiadali Fathima, C. Sanjeeviraja, G. Kalai Selvan, S. Arumugam, and R. Kalai Selvan, *Mater. Res. Bull.* 48, 1110 (2013).
24. POWDMULT: An Interactive Powder Diffraction Data Interpretation and Indexing Program Version 2.1, E. Wu, School of Physical Sciences, Flinders University of South Australia, Bradford Park, SA 5042, Australia.
25. M.A. El-Fattah Gabal, Y.M. Al Angari, and A. Yousef Obaid, *C. R. Chim.* 16, 704 (2013).
26. S.-H. Chuang, M.-L. Hsieh, and D.-Y. Wang, *J. Chin. Chem. Soc.* 59, 628 (2012).
27. R. Vijayalakshmi and V. Rajendran, *E-J. Chem.* 9, 282 (2012).
28. K.K. Bamzai, V. Gupta, P.N. Kotru, and B.M. Wanklyn, *Ferroelectrics* 413, 328 (2011).
29. L.L. Hench and J.K. West, *Principles of Electronic Ceramics* (New York: Wiley, 1990), p. 189.
30. J.C. Anderson, *Dielectrics* (London: Chapman and Hall, 1964).
31. P. Ganguli, S. Devi, A.K. Jha, and K.L. Deori, *Ferroelectrics* 381, 111 (2009).
32. P. Kumar, S. Singh, J.K. Juneja, C. Prakash, and K.K. Raina, *Ferroelectr. Lett.* 37, 110 (2010).
33. J. Rout, B.N. Parida, P.R. Das, and R.N.P. Choudhary, *J. Electron. Mater.* 43, 732 (2014).
34. R.N.P. Choudhary, C. Behera, P.R. Das, and R.R. Das, *Ceram. Int.* 40, 12253 (2014).
35. M.A.L. Nobre and S. Lanfredi, *J. Appl. Phys.* 93, 5557 (2003).
36. D.K. Pradhan, R.N.P. Choudhary, C. Rinaldi, and R.S. Katiyar, *J. Appl. Phys.* 106, 024102 (2009).
37. C. Behera, P.R. Das, and R.N.P. Choudhary, *J. Electron. Mater.* 43, 3539 (2014).
38. T. Badapanda, V. Senthil, S.K. Rout, S. Panigrahi, and T.P. Sinha, *Mater. Chem. Phys.* 133, 863 (2012).
39. B. Behera, P. Nayak, and R.N.P. Choudhary, *J. Alloys Compd.* 436, 226 (2007).
40. S. Dash, R. Padhee, P.R. Das, and R.N.P. Choudhary, *J. Mater. Sci.: Mater. Electron.* 24, 3315 (2013).
41. A.K. Jonscher, *Nature* 267, 673 (1977).
42. B. Pati, B.C. Sutar, B.N. Parida, P.R. Das, and R.N.P. Choudhury, *J. Mater. Sci.: Mater. Electron.* 24, 1608 (2013).
43. N.F. Mott and E.A. Davis, *Electronic Processes in Non-crystalline Materials*, 2nd ed. (Oxford: Clarendon, 1979).
44. G.V.S. Murthy, N. Parveen, and C.R.V.S. Nagesh, *International Mineral Processing Congress, Paper No. 1016.*
45. J. Mona, S.N. Kale, A.B. Gaikwad, A. Vadivel Murugan, and V. Ravi, *Mater. Lett.* 60, 1425 (2006).
46. A.T. Raghavender, N.H. Hong, K.J. Lee, M.-H. Jung, Z. Skoko, M. Vasilevskiy, M.F. Cerqueira, and A.P. Samantilleke, *J. Magn. Magn. Mater.* 331, 129 (2013).
47. A.M. Áŕevalo-Ĺopez and J.P. Attfield, *Phys. Rev. B* 88, 104416 (2013).
48. M. Enhessari, A. Parviz, E. Karamali, and K. Ozaee, *J. Exp. Nanosci.* 7, 327 (2012).
49. R.S. Singh, T.H. Ansari, and R.A. Singh, *Proc. Indian Natl. Sci. Acad.* 61, 425 (1995).
50. B. Zhang, T. Katsura, A. Shatskiy, T. Matsuzaki, and W. Xiaoping, *Phys. Rev. B* 73, 134104 (2006).